Materials Science & Engineering C 94 (2019) 417–425

Contents lists available at ScienceDirect

Materials Science & Engineering C

journal homepage: www.elsevier.com/locate/msec

Towards the production of natural rubber-calcium phosphate hybrid for applications as bioactive coatings

Rodney Marcelo do Nascimento[a,*], Amauri Jardim de Paula[b], Naiara Cipriano Oliveira[b], Ana Cecilia Alves[b], Yasmine Maria Lima de Oliveira Aquino[b], Antônio Gomes Souza Filho[b], João Elias Figueiredo Soares Rodrigues[a], Antônio Carlos Hernandes[a]

[a] São Carlos Institute of Physics, University of São Paulo, USP, PO Box 369, 1356-6590 São Carlos, SP, Brazil
[b] Departamento de Fisica, Universidade Federal do Ceara, P.O. Box 6030, 60455-900 Fortaleza, CE, Brazil

ARTICLE INFO

Keywords:
Charged particles
Body fluid
Vibrational spectroscopy
Electronic microscopy

ABSTRACT

This paper assesses the morphological, structural and bio-physicochemical stability of natural rubber (NR) *Hevea brasiliensis* coatings incorporated with microparticles of calcium phosphate-based (CaP) bioactive ceramics. Optical and electronic spectroscopic imaging techniques were employed to successfully evaluate the NR encapsulation capability and the stability of the coating in a biologically relevant media for bio-related application, i.e., simulated body fluid (SBF). The chemical structure of the natural polymer, the microchemical environment at the NR-CaP interface and the morphology of the CaP clusters were fully characterized. Further, the response of the hybrid coating to SBF was evaluated by incubating the samples for 30 days. The hybrid coating formed on Si surface (inert substrate) exhibited both stability and biodegradability in different levels (time dependence), thus opening horizons for applications as coatings for both biomaterials and drug delivery systems.

1. Introduction

Natural rubber (NR) obtained from the *Hevea brasiliensis* latex is highly demanded by manufacturing industry because it has superior properties as compared with the synthetic rubber. However, in order to expand the potential for new applications, the development of novel composites combining NR with other materials is a current target of many investigations [1–3]. These hybrid systems usually present new and superior properties to this fine NR. For instance, a NR-graphene composite has been studied in order to obtain a material with high electrical conductivity combining the flexibility properties of the polymer [4]. In another hand, a promising field for application of the NR-based materials is in biomedicine [5–15].

A great potential lies on calcium phosphate-NR composites and hybrids materials, especially for applications as (or associated with) implants. However, prior to achieving commercial products, one must elucidate relevant aspects related to the processing of NR for the production of biomaterials or composites for such biomedical applications. An issue to be clarified includes the possible effects of the ammonia content (used to avoid clotting and it is very important for the preservation of the latex [16]) on the morphology and structure of NR particles present in the cream phase. Additionally, in composites, the molecular interactions between non-rubber constituents of the NR cream and charged particles were not properly described so far. In the case of CaP charged particles dispersed in NR phase, the suggestion of the homogeneous and random distribution of different molecular groups correlated with two emission bands in the photoluminescence spectrum are not reproducible for attesting the protein-phospholipids heterogeneous distribution models [17–19]. In this way, new techniques and approaches are required to improve the hybridization of the NR looking to fully exploit the polymeric matrix to design a functional material with optimized properties.

Recently, we have described the production of membranes of NR-CaP hybrids formed from casting methods using bioceramic CaP particles dispersed in NR colloidal suspensions [20]. The membranes conjugated the favorable biocompatible properties of CaP with the renewable and low-cost characteristics of NR. Here, we describe the production and characterization of coatings formed from NR-CaP hybrids and their physicochemical stability in the presence of a simulated body fluid (SBF), which has a high relevance towards the development of implants coatings. By applying physico-chemical assays, vibrational and electronic spectroscopic imaging techniques, we assessed morphological and structural aspects of the processed NR prior and after to the incorporation of CaP. The influence of ammonia content on the final

* Corresponding author.
E-mail address: rodneymn@ifsc.usp.br (R.M. do Nascimento).

https://doi.org/10.1016/j.msec.2018.09.048
Received 13 December 2017; Received in revised form 5 August 2018; Accepted 18 September 2018
Available online 19 September 2018
0928-4931/

products was investigated. The organic-inorganic interfaces of the NR-CaP hybrid were characterized by molecular spectroscopy as well. We investigated the functional chemical groups responsible for forming the core-shell structure that traps the bioceramics (CaP). The chemical structure of the natural polymer, the microchemical environment at the NR-CaP interface and the morphology of the CaP clusters were fully described. In view of biomedical applications of the NR-CaP hybrid, we evaluated the response of the NR-CaP coating exposure to SBF by incubation of the samples for 30 days. The remarkable stability of the coating on Si substrate and its surface modifications by exposure to the biological environment, as well as the biodegradability in different levels regarding time dependence, are discussed aiming the possible applications in the biomedical field, such as coatings for biomaterials and drug delivery systems.

2. Experimental procedures

2.1. Separation of the natural rubber cream

Samples of natural rubber latex (NR) were collected from *Hevea brasiliensis* trees (clone RRIM 600) located at Estância Regina farm, São Paulo, Brazil (see Fig. 1), immediately transferred to propylene tubes containing different ammonia content, which led to final concentrations of 0.3%, 0.5%, 0.7%, 0.9% w/w (denoted sample as NR 0.3A, NR 0.5A, NR 0.7A and NR 0.9A, respectively) and stored under refrigeration at 4 °C to avoid microbial contamination. Initially, aliquots of 1.5 mL of each sample with different ammonia content were added to a 2 mL microcentrifuge tube and then centrifuged for 90 min at 24 °C in an Eppendorf 5418 R centrifuge. For each sample, four different centrifugation speeds were employed: 2000*g*, 6000*g*, 10000*g* and 14000*g*. After centrifugation, the microtubes were photographed with a Nikon D3200 camera to compare the effect of centrifugation speed in phase separation. Fig. 1 shows the typical appearance of centrifuged NR latex: cream phase (A) contains the concentrated natural rubber particles; serum fraction (B) with high water ratio, as well as rubber particles and non-rubber components; and (C) contains the lutoids [21]. After separation, a part of the resulting upper phase (cream) from the samples centrifugated at 2000*g* was collected with a spatula and re-dispersed in deionized water for the analysis of the particle size through the dynamic light scattering (DLS). Dispersions were obtained at ~0.011% (w/w) in deionized water, and DLS measurements were performed on a Zetasizer Nano ZS (Malvern Instruments Ltd., Malvern, UK).

NR samples were investigated by Attenuated Total Reflection Fourier Transform Infrared (ATR-FTIR) spectroscopy to verify if their structures are modified by ammonia content and centrifugation process. ATR-FTIR spectra were recorded with OPUS software on a Bruker Vertex 70v spectrometer. The system was equipped with a Globar source used to Middle Infrared Region (MIR) and a detector DLaTGS. ATR-FTIR spectra were recorded in the range of 4000–1400 cm^{-1} with a resolution of 2 cm^{-1}. The background was measured before testing each sample. For each sample, one spectrum was recorded on five different regions. Each spectrum was obtained from 256 successive scans. The final ATR-FTIR spectra are the average of five spectra acquired at different regions of the sample. This first assessment provided the parameters to enrich the cream fraction with NR, and to decrease the amount of water in the dried NR (after centrifugation).

2.2. Production of NR-CaP hybrid coatings

NRs were extracted by centrifugation at 14,000*g* for 90 min. Then NR cream was dried at 45 °C for 24 h, and then re-suspended in chloroform for 2 days. Powders of a CaP-based bioactive ceramic (cell viability on CaP coatings was described elsewhere by our group [22]) containing Ca_5P_8 (47.8 wt%), $Ca(PO_4)_3OH$ (9.5 wt%), $CaCO_3$ (36.3 wt %), and Ca (6.3 wt%) were mixed in the NR cream solution (in chloroform) under magnetic stirring for 30 min.

In addition, silicon substrates of 5 × 5 mm^2 with polished surfaces were sequentially cleaned in an ultrasonic bath with acetone, isopropyl alcohol and ultrapure water (for 15 min each step), and finally dried at 50 °C for 10 min. NR and NR-CaP suspensions in chloroform (30 μL) were controllably deposited on silicon substrates and the substrates were dried for 12 h at 60 °C, thus generating coating samples Si/NR and Si-NR/CaP. The charge effects were evaluated through determination of the polar component of the free energy γ_s^p using the followed liquids: ultra-pure water (γ^p = 51 mJ/m2, γ^d = 21.8 mJ/m^2 and γ = 72.8 mJ/m^2), formamide (γ^p = 18.5 mJ/m^2, γ^d = 39.5 mJ/m^2 and γ = 58 mJ/m^2), ethylene-glycol (γ^p = 19 mJ/m^2, γ^d = 29 mJ/m^2 and γ = 48 mJ/m^2), di-iodomethane (γ^p = 0 mJ/m^2, γ^d = 50.8 mJ/m^2 and γ = 50.8 mJ/m^2) and hexadecane (γ^p = 0 mJ/m^2, γ^d = 27.47 mJ/m^2 and γ = 27.47 mJ/m^2. From measurements of contact angles, we obtain the plot of $0.5\gamma_L(1 + \cos\theta)$. $(\gamma^d)^{-1/2}$ versus $(\gamma^p/\gamma^d)^{1/2}$ for the determination of the polar component of free energy γ_S^p.

2.3. Incubation in simulated body fluid

The SBF medium was obtained with the dissolution of 0.2 g KCl, 8.0 g NaCl, 0.2 g $CaCl_2 2H_2O$, 0.05 g NaH_2PO_4, 1.0 g $NaHCO_3$, 0.1 g $MgCl2{\cdot}6H_2O$ and 1.0 g glucose in 1 L of ultrapure water at a constant pH (7.45). We evaluated two protocols for this study aiming an optimization and reproducibility of the results and this protocol was chose to prevent early nucleation and precipitation of salts. Both the coatings (NR and NR-CaP) and the SBF medium were sterilized in UV for 15 min before the experiments. A control clean Si substrate (without coating) was also used. All substrates were weighted in an analytical balance before each experiment. Samples were then immersed in wells containing 5 ml of SBF and kept at 37.5 °C for different periods of time, i.e. 1, 15 and 30 days. After every time intervals, the substrates were collected, gently cleaned in ultrapure water, dried in a dissector for 24 h, and finally measured in the balance. Coatings for Si, Si/NR and Si/NR-CaP were labeled as function of time (#1, #15 and #30), totalizing nine groups of surfaces. After the removal of the samples from SBF, the medium just for samples #30 (with 30 days of immersion) was evaporated up to the volume of 0.5 mL, then dripped on glass slides and dried at 37 °C. These three new samples (SBF/Si, SBF/Si/NR and SBF/Si/NR-CaP) were analyzed in regard to their composition. The SBF immersion experiments were repeated at least 5 times, and the results are provided as mean values and standard deviation. For each day (1, 15 and 30), samples of Si, NR and NR-CaP were compared by the Kruskal-Wallis statistical approach.

2.4. Physical and chemical characterizations

Confocal Raman spectroscopy and Raman spectral mapping were employed to probe the phase of the encapsulated particles of the hybrid NR-CaP through XYZ profiles of the vibrational bands. The spectra and the Raman spectral mapping were obtained by using a microscope WITec *alpha* 300 equipped with a linear stage, piezo-driven, objective lens Nikon 20× (NA = 0.46) and 100× (NA = 0.8) and polarized laser with 514 or 632 nm wavelengths. The Raman light was detected by a high-sensitivity, back-illuminated spectroscopic CCD after being dispersed by a 600 grooves/mm grating. The organic-inorganic interface was investigated by Raman mappings from XY depth profiles in two planes (Z = 0 and Z = 2.6 μm) carried out in a region of 30 × 30 μm^2 with 60 points per line and 60 lines per image. The integration time for each point was 0.5 s and all mapping were performed at room temperature.

Both NR samples and dried SBF were analyzed by scanning electronic microscopy (SEM) and energy dispersive X-ray spectrometry (EDS) in the large-field scan. The experiments were carried out in the electron microscope Quanta-450 (FEI) with a field emission gun, a 100 mm stage, and X-ray detector model 150, Oxford. An overlapping of areas of adjacent images acquired independently after x-y

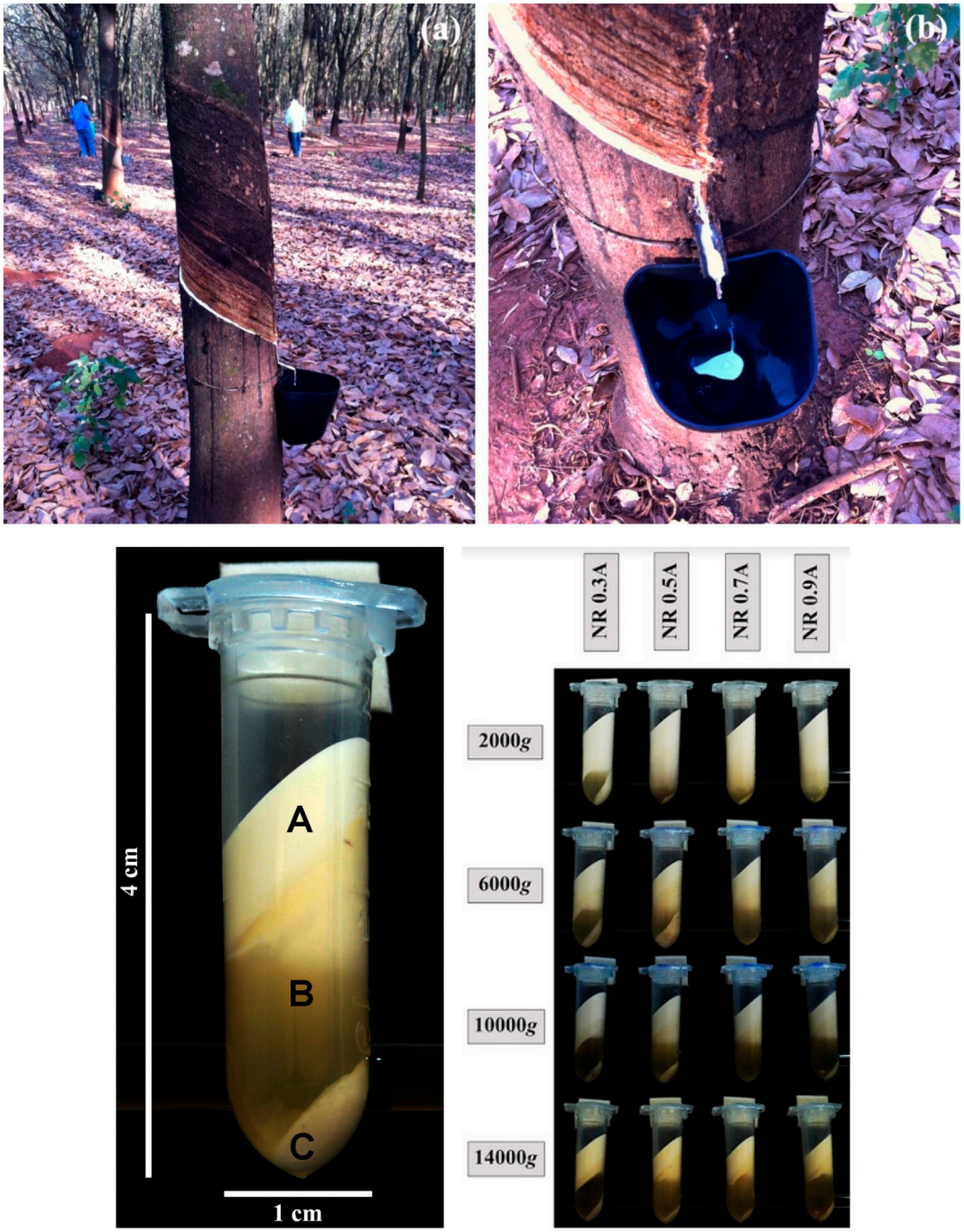

Fig. 1. Latex collection and separation process: lateral view of the latex collection from the *Hevea brasiliensis* tree, front view of the latex collection in an appropriate flask, visual presentation of latex after centrifugation showing (A) cream fraction, (B) serum fraction (C) lutoids at different ammonia concentration and centrifugal forces.

movements of the microscope stage were performed for the generation of the large-field images.

3. Results and discussion

3.1. Morphological and structural assessment of NR particles

The fresh latex as extracted from the tree is very susceptible to microbial contamination. For this reason, ammonia is added to latex in order to increase the pH and, therefore, to decrease microbial activity and prevent the latex coagulation even when stored for a long time (more than a year). In order to check how ammonia affects the cream chemical structure and the NR particles morphology, samples NR 0.3A, NR 0.5A, NR 0.7A and NR 0.9A were submitted to different centrifugal forces. The sample consisting of 0.3% w/w ammonia (NR 0.3A) shows a larger cream phase in all centrifugations, evaluated in terms of volume in the microtube. On the other hand, samples NR 0.5A, NR 0.7A and NR 0.9A show a similar cream volume. At 2000*g*, the cream phase area is larger when compared to the other samples. At 6000*g*, 10,000*g*, and 14,000*g*, however, the cream phase remains approximately the same regarding its volume. In addition, a low centrifugal force leads to a high turbidity level in the serum phase, while a high centrifugal force leads to transparent serums (see Fig. 1). These results indicate a better separation of the organic (NR) and liquid (serum) phases occurring at

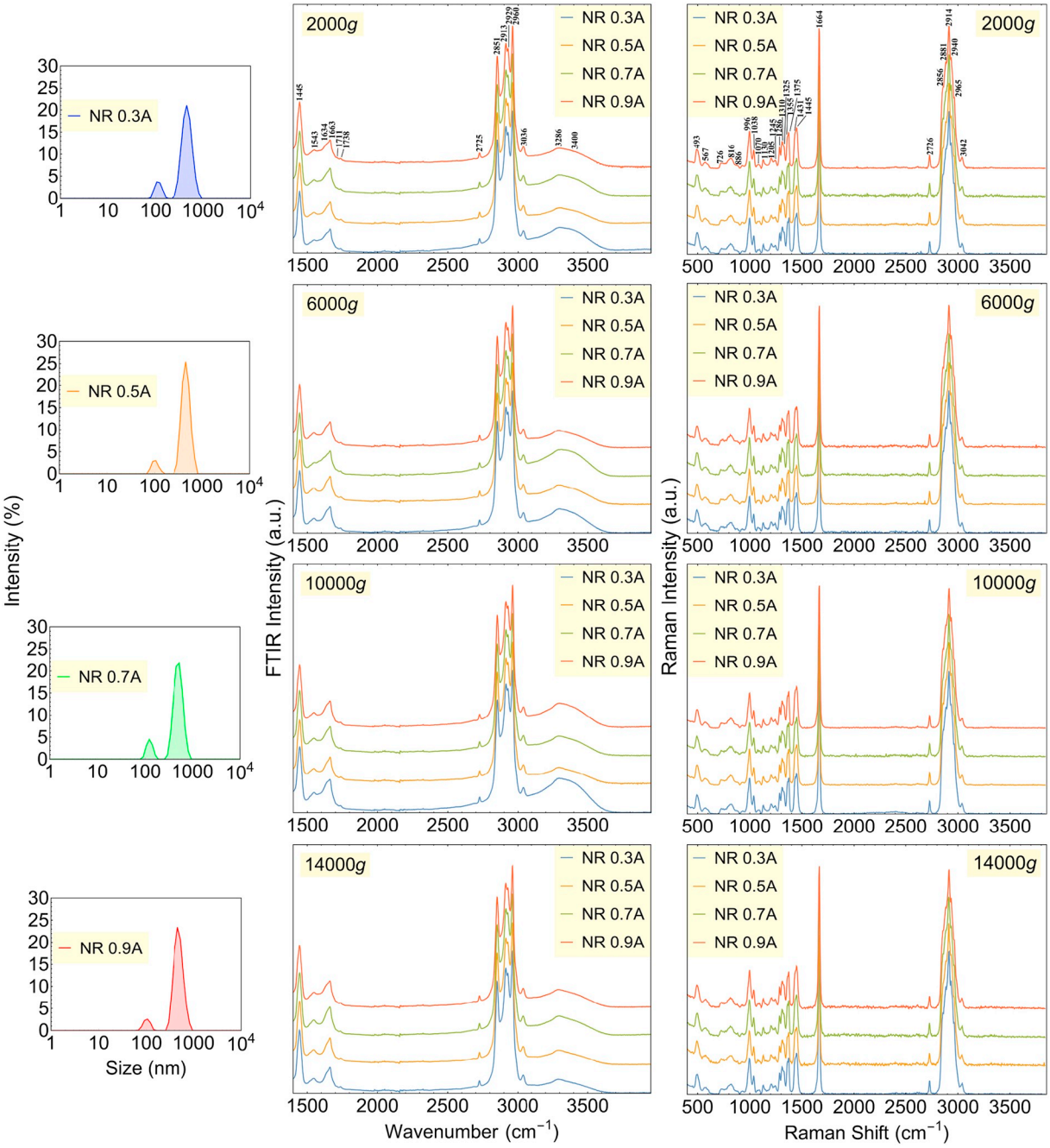

Fig. 2. Dynamic light scattering results of the NR samples with different ammonia concentrations (a). Comparison of ATR-FTIR (b) and Raman (c) spectra of cis-1,4-polyisoprene of NR samples with different ammonia concentrations obtained from different centrifugation velocities. Each spectrum showed in panels (b) and (c) represents the average between three different spectra for each sample (see Supplementary tables).

14,000*g*. Fig. 2(a–d) shows the results of DLS performed on the sample, which exhibited bimodal distributions of particle size ranging from 60 to 190 nm and 220–1000 nm. From the results collected from all samples, it was observed that the variation of the ammonia concentration did not significantly change the final particle size distribution.

Fig. 2 displays the comparison of ATR-FTIR and Raman spectra of cis-1,4-polyisoprene of NR samples (i.e. centrifuged and dried cream phase) with different ammonia concentrations obtained from different centrifugation forces. Both ATR-FTIR and Raman spectra exhibited the same characteristic bands of the NR macromolecular structure, regardless of the ammonia content and centrifugation velocities. Spectra of some non-isoprene compounds of cis-1,4-polyisoprene show bands at 1665 cm^{-1} which refer to specific functional group related to the existence of protein material [23,24]. Two bands were observed for all the NR samples between 3500 and 3200 cm^{-1}. The 3400 cm^{-1} band was assigned to stretching vibration of water, which might be related to protein structure [25]. An N—H stretching band at 3283 cm^{-1} is assigned to amines coming from the proteins. The 1738 cm^{-1} band was assigned to carbonyl stretching band related to ester groups, and can be ascribed to hydrogen bonded species [23] and band at 1711 cm^{-1} band was assigned to carbonyl stretching of carboxyl groups. The bands at 1630 and 1541 cm^{-1} (amide I and amide II, respectively) were attributed to NR proteins and polypeptides, which come from peptide bonds [24,25]. The complete positions and assignments of bands observed in ATR-FTIR and Raman spectra of NR samples are provided in supplementary tables. By considering these results of the volume of the cream

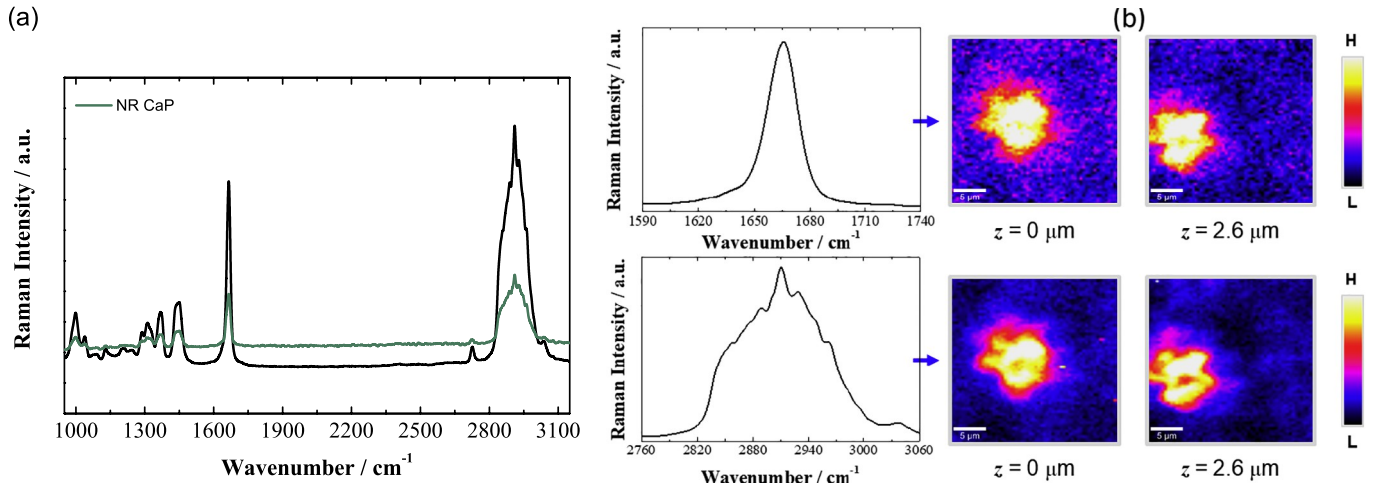

Fig. 3. Characterization of hybrid NR-CaP: Raman spectra obtained with λ = 514 nm excitation at room temperature before (black) and after (green) CaP incorporations (a), Raman Spectral – mapping obtained from x,y depth profiles with plan z = 0 (top of the cluster) and −2.6 μm. Intensity profiles were acquired by considering the peaks at 1665 cm^{-1} and 2900 cm^{-1} with objective lens 20× (b). Color scale in panels varies from lowest (L) to highest intensity. (For interpretation of the references to color in this figure legend, the reader is referred to the web version of this article.)

phase (larger for NR 0.3A centrifuged at 14,000*g*), the morphology of NR particles (similar to all ammonia concentration), and the chemical structure of the dried cream phase (similar to all ammonia concentration and centrifugation velocities), we used for preparing the NR-CaP composites NR extracted from raw latex suspensions conserved at 0.3% of ammonia (w/w) and centrifuged at 14,000*g* for 90 min.

3.2. Characterization of the NR-CaP and its encapsulation properties

We investigated the NR encapsulation capability in order to apply NR-CaP as functional coating on biomaterials by monitoring the molecular fingerprint of the NR after the incorporation of CaP bioceramic particles. Fig. 3(a) shows the Raman spectra acquired by using λ = 514 nm excitation, at room temperature, before and after CaP incorporations into NR polymer. The presence of the CaP particles seems to not affect the main chemical groups of the NR matrix. Raman spectra of the samples exhibited the characteristic peaks of the NR macromolecular structure, along with peaks from water molecules adsorbed/incorporated in the matrix, and also related to calcium phosphate vibrational modes. The bands in 2820–3030 cm^{-1} spectral range are assigned to C—H stretching from CH_2 and CH_3 [26], characteristic of *cis* poly isoprene chain groups. In addition, this is a spectral region of phospholipidic chains characterized by symmetric and antisymmetric stretching modes, and enhanced by Fermi resonance [27–29]. This spectral region also exhibits C—H stretching vibrational bands of aminoacids, related to the presence of protein structures incorporated in the NR matrix. However, considering the concentration of the abovementioned consituents, the major contribution for 2820–3030 cm-1 bands is from NR. The band in 1660–1680 cm^{-1} region is assigned to C = C stretching, characteristic vibration of hydrocarbons. The bands at 1450 cm^{-1} and 1300 cm^{-1} are assigned to C—H deformation mode and ring vibrations twisting (t(CH_2)) [27], respectively. Ring vibrations are a characteristic of Amide II-III, also present in the protein structures and associated with coupled C—N stretching and N—H bending vibrations [30]. The bands at 1000 cm^{-1}, attributed to breathing mode of the phenylalanine-aromatic amino acids as well as P—O stretching mode, will be discussed in more detail later on.

Fig. 3(b) displays a Raman spectral mapping collected from XY depth z profiles of a NR-CaP cluster. Intensity profiles were acquired with bands centered at 2912 cm^{-1} (a) and 1665 cm^{-1} (b). The images revealed details of the chemical distribution in which the shell is exposed on the surface. The C—H stretching is observed in the center of the cluster with highest intensity. Such center appears an irregular shape that fits with the CaP particle shapes. The particles were "sliced" by the confocal plane of the surface (*xy*) and in across section μm from the top of the clusters were revealed. The molecular fingerprint is attributed to a core-shell structure comprised of isoprene molecules, surrounded by layers of proteins (~85%) and phospholipids (~16%) [10,16], whereby the trapped process is attributed to the attraction between non-rubber particles and CaP during the material processing. As a consequence, the encapsulation process induces a reduction of the surface charge in 35%, as attested by the decrease of the polar component of free energy γ_S^P.

3.3. Surface characteristics of the NR and NR-CaP coatings in SBF

Fig. 4(a) depicts the SEM micrographs coatings before and after immersion in SBF for different exposure time. It can be observed that a growth orientation of salt particles from SBF was formed on coatings, and the increase of the amount of particles was proportional to the time of exposure to SBF. Fig. 4(b) displays the Raman spectra of the samples before and after soaked in SBF in different periods of time. As observed, the NR preserved its chemical structure along the time in contact with SBF, i.e., the coating resists to the high ionic strength of the SBF medium. On the other hand, a new Raman band appeared in the 900–1070 cm^{-1} region, whose intensity increases as a function of the time to SBF. Fig. 4 (c) displays the Lorentzian decomposition of the spectra of the NR coatings. The shoulder at 944 cm^{-1} becomes prominent after interacting 30 days with SBF. Such region is associated with internal vibrations of the PO_4 unit, and the peak is a result of the salt precipitation on the coating. Strictly speaking, the band in Raman spectrum is attributed to stretching $PO_4^{3-}\nu_1$, one of four normal modes groups of the regular free phosphate tetrahedron [31], which is a characteristic of a highly disordered or amorphous calcium phosphate [32]. Furthermore, the spectrum deconvolution revealed changes in the 982 cm^{-1} region that was attributed to P—O stretching, thus indicating the presence of other calcium phosphate phases such as dicalcium phosphate dehydrate [33]. In addition, changes in this band region may induce the formation of magnesium potassium phosphate hexahydrate [31] and/or magnesium phosphate tribasic [$Mg_3(PO_4)_2$] [34]. By combining vibrational and electronic spectroscopy techniques, we have observed a large among of Ca and Mg on NR after the SBF immersion experiments.

It is worth noticing the inversion in the intensity of the main Raman peaks (2915 cm^{-1} and 1665 cm^{-1}) due to a decrease in the C—H stretching signal. Moreover, a decrease in the percentage of carbon

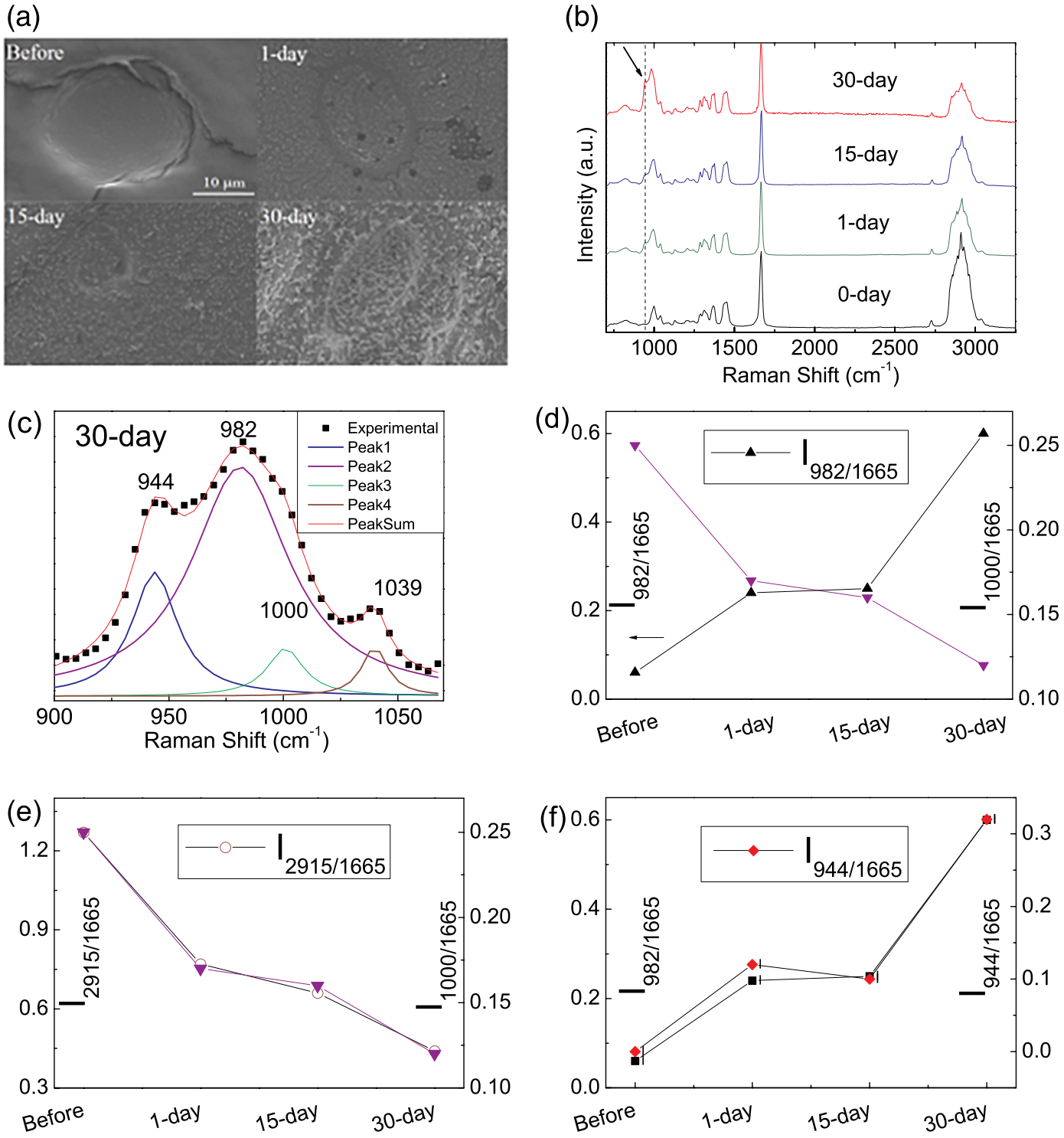

Fig. 4. SEM images (a) and Raman spectra (b) of the NR coating before and after exposure to SBF for different times. Lineshape analyses of the Raman spectra (c) and normalized intensities (I) of the 900–1060 cm^{-1} band regions of the NR coatings (d–f).

followed by an increase in the percentage of oxygen was detected in the samples after interaction with SBF, as attested by EDS (chemical color maps are provided in Fig. 5). Bands in the 900–1070 cm^{-1} region were normalized by the peak of the intense C═O stretching rocking signal observed at 1665 cm^{-1} in order to confirm no independence of both the laser power and signal collection efficiency. We found modifications in the PO_4 structures through the evolution of the intensity ratios I_{band}/I_{1665}, i.e., I_{2915}/I_{1665}, I_{1000}/I_{1665}, and I_{944}/I_{1665} within 30 days (Fig. 4d–f). This result confirms the increased amount of particles due to the formation of newly deposited minerals, especially calcium and magnesium phosphates, which are well-known functional materials for tissue regeneration. SEM images showed in Fig. 5 confirm the stability of the NR-CaP coatings before and after exposure to SBF until 30 days.

3.4. Biodegradability of the NR coatings in simulated body fluid (SBF)

Statistical analyses revealed no difference in the values of mass of the coatings after 1 day in SBF (see Sup. Fig. 3). Both Si/NR and Si/NR-CaP

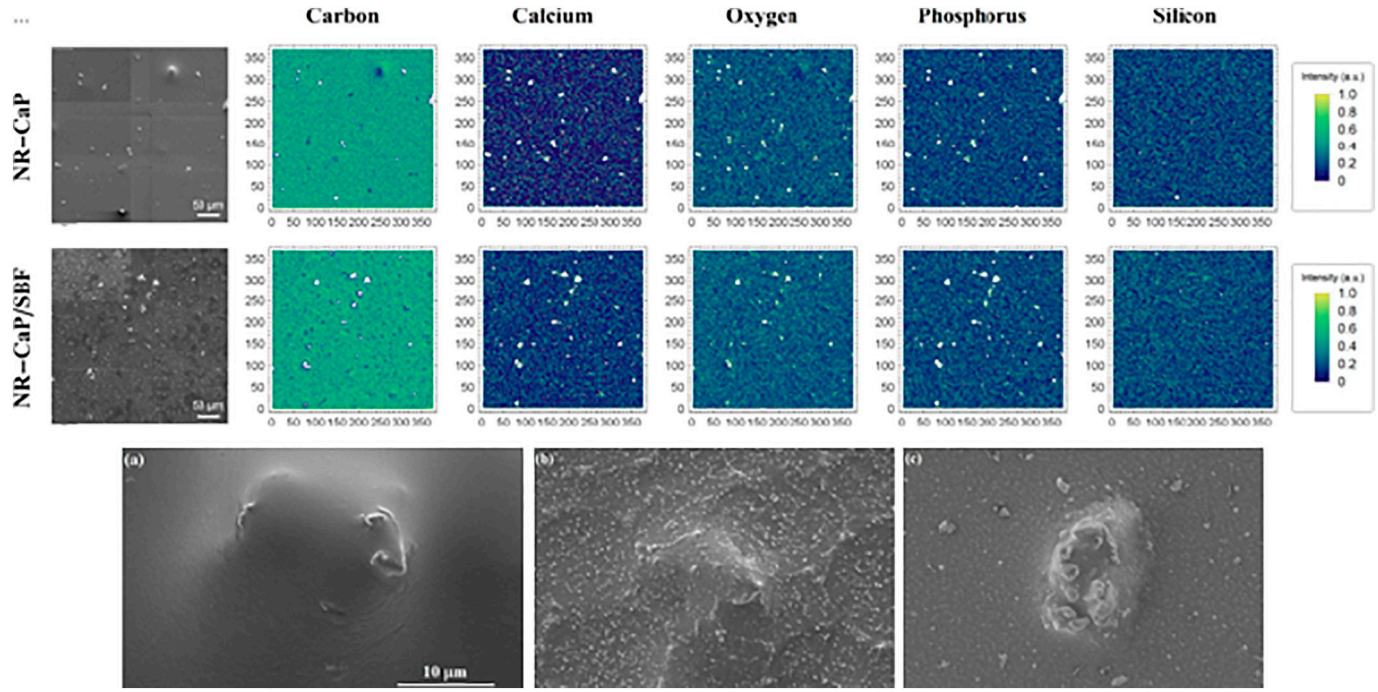

Fig. 5. EDS chemical color maps of Si/NR-CaP coatings before and after exposure to SBF. SEM images of Si/NR-CaP coatings with an encapsulated CaP obtained before exposure to SBF (a), after exposure for 1 day (b) and 30 days (c).

samples exhibited similar physicochemical stability behavior in the SBF for all incubation times analyzed. On the other hand, results of the mass measurements indicated a reduction in mass for the coatings between 1 and 15-days in the fluid, although no significant difference was found for 15 and 30-days. Taking into account the error bars for silicon substrate (control), the values of mass appear to be constant between 15 and 30 days. We can think of two mechanisms that may be responsible for such behavior: (i) releasing of material from coating to the fluid and (ii) deposition of material from fluid to coatings. For both, the values of mass of the samples for different periods of time are no more comparable.

Since the modifications in the NR coatings are being attributed to the aggregation of particles originated from the fluid, it is relevant to probe its effects on SBF. Fig. 6 shows the SEM micrographs with their respective chemical color maps of the dried SBF_{Si} (a), $SBF_{Si\text{-}NR}$ (b) and $SBF_{Si\text{-}NR\text{-}CaP}$ (c) after 30 days. For the experiments, the final SBF medium without NR samples was used as a control for comparisons. We found a different percentage of carbon, from 4.8% (SBF_{Si}) to 10.9% in $SBF_{Si\text{-}NR}$ and 9.7% in $SBF_{Si\text{-}NR\text{-}CaP}$. It is a good agreement with the decrease in the percentage of carbon observed in the NR sample after 30 days exposed in SBF (from 84.2% to 72.4%). Such result suggests that the coatings exhibit a level of biodegradability with liberation NR from surfaces to SBF. On the other hand, no variation in the percentage of phosphorous was observed, thus indicating that the formation of calcium phosphate particles on the NR coatings is due to the electrostatic interaction between negatively charged layer along the NR surface (~ -57 mV) and Ca^{2+}. The deposited calcium ions, in turn, interacted with phosphate ions (PO_4^{3-}) in the SBF. Such result suggests that certain level of the negative surface charges is responsible for the adsorption of Ca^{2+} and Mg^{2+} from SBF. The origin of such charges is on non-rubber particles. Therefore, the inorganic components were embedded on the coatings by ionic bonds. The biological fluid contains varying amounts of cations and anions responsible to different biological properties, such as tissue regeneration-mineralization of the bone. We found a decrease of the calcium in dried SBF_{NR} during interaction with the coating, i.e.; from 5.2% to 1.4% and 1.7%, for SBF_{NR} and $SBF_{NR\text{-}CaP}$, respectively. In the same way, we detected a decrease of the magnesium from 4.2% to 1.0% for SBF_{NR} and 1.1% for $SBF_{NR\text{-}CaP}$ system. The cationic adsorption process by a negatively-charged surface explains the surface modifications of the coatings by the biological environment. By combining the vibrational-electronic spectroscopies analyses according to described in Sections 3.3 and 3.4, it is clear that the NR-CaP coatings present both bio mineralization kinetics and biodegradability properties.

3.5. Cell viability of the NR-CaP surfaces

The biocompatible performance of the materials was investigated through quantitative analyses of stem-cells response on hybrid NR. The experiments were carried out at *Biomatériaux et Inflammation en Site Osseux, Pôle Santé, UFR d'odontologie* of the *Université of Reims*. The protocol used in the experiments with Wharton's jelly stem cells, in accordance with the usual ethical legal regulations, was recently described by the team [35]. Fig. 7 shows the average results of the growth of stem cells on the surfaces. The statistical analyses of the cell viability of samples by Mann-Whitney revealed no significant difference between NR surfaces and control group for 48 h ($p = 0.1075$), and one week ($p = 0.9353$). The material exhibited 100% of cell viability in comparison with the control group after one week.

Biomaterials based on natural rubber may have limitations application if they are not properly processed. Factors such as the amount of ammonia and the method of harvesting the matrix from the trees can affect the cellular response [13]. Allergenic effects are the most serious complications in the utilization of the latex as biomaterials. FDA estimates that 1 to 6% of the general population may be sensitive to natural rubber latex. In fact, Latex is a very rich biological medium with over 200 different types of proteins. Only 13 of them are allergenic and can be harmful to health. Therefore, in order to profit the benefits of this natural polymer in biomedicine, there are two possibilities: 1) removal of non-rubber particles or 2) inhibition of their activities. In some previous experiments, we have removed the proteins from the latex by centrifugation process. However, a noticing decrease in the adhesion and stability of the latex film was observed. Herein, we propose a hybrid NR by incorporation of CaP particles in order to reduce the effects of the negative charge of surfaces rather than removing the proteins, since the removal of the proteins results in limitations on the mechanical and superficial properties. The inhibition of the activity of the proteins can be considered the vanguard of the options for diminishing the undesirable effects of the latex, such as the treatment of natural rubber with vegetable tannin [36] where the researchers have

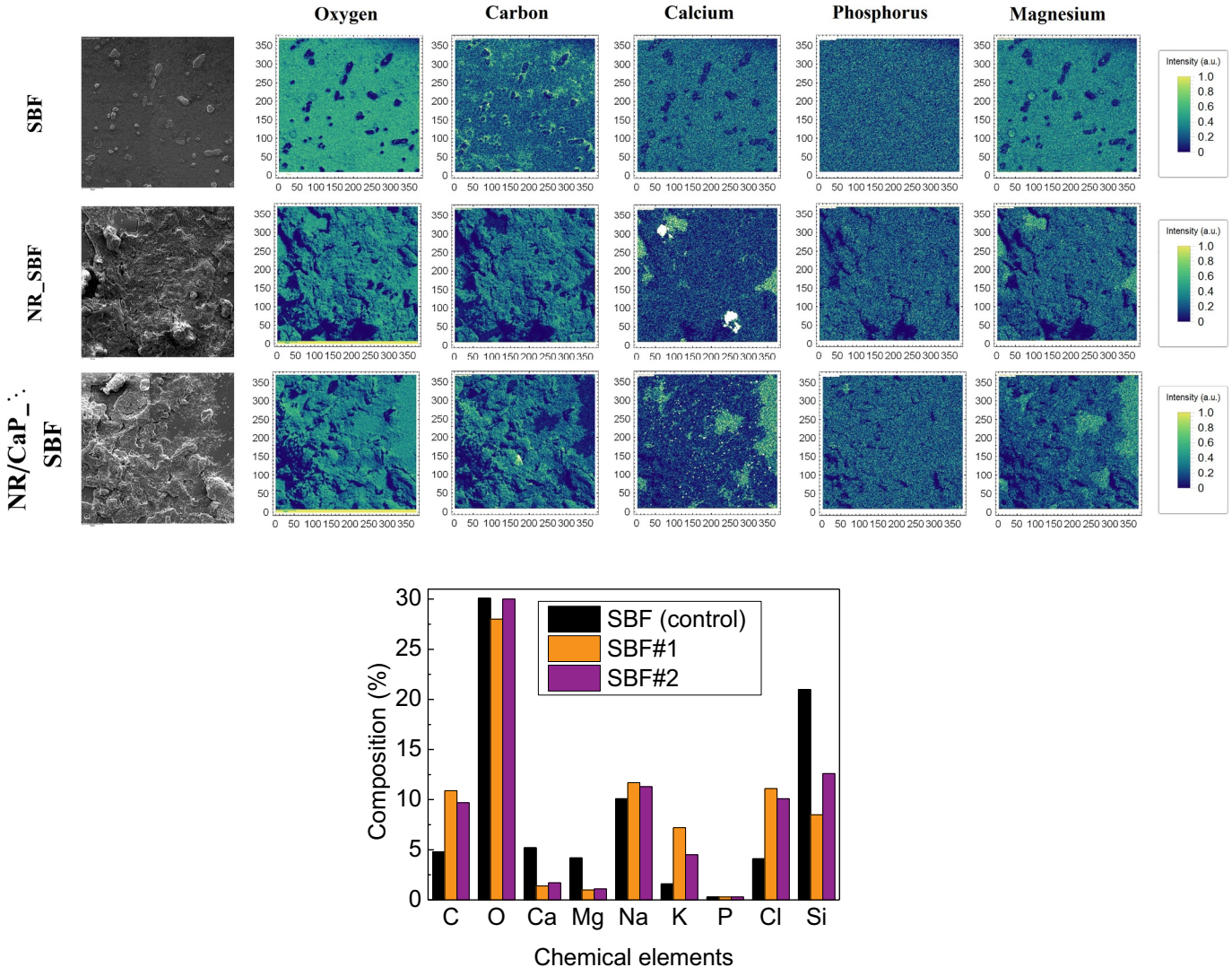

Fig. 6. SEM micrographs, chemical color maps and semi-quantitative chemical composition of the dried SBF_{Si} (a), $SBF_{Si\text{-}NR}$ (b) and $SBF_{Si/NR\text{-}CaP}$ (c) after soaking experiments for 30 days.

developed a way to inactivate allergenic proteins in natural rubber latex by using tannin as a surface coating. The hybridization process of the NR polymer as proposed in this work decreases the negative charges of proteins from −57 mV to ~ −15 mV, as attested by the zeta potential measurements. The resulting charge of the hybrid NR is slightly lower than a cell membrane, which consists of phospholipid bilayers with charge ~ −20 mV. A slightly negatively charged molecules show a lower unfavorable effect on cell response as demonstrated in [37]. Therefore, we have attributed the good cell viability of the hybrid NR to the decreasing of charge effects of the proteins on NR surfaces.

4. Conclusions

We have studied the production of coatings of natural rubber-calcium

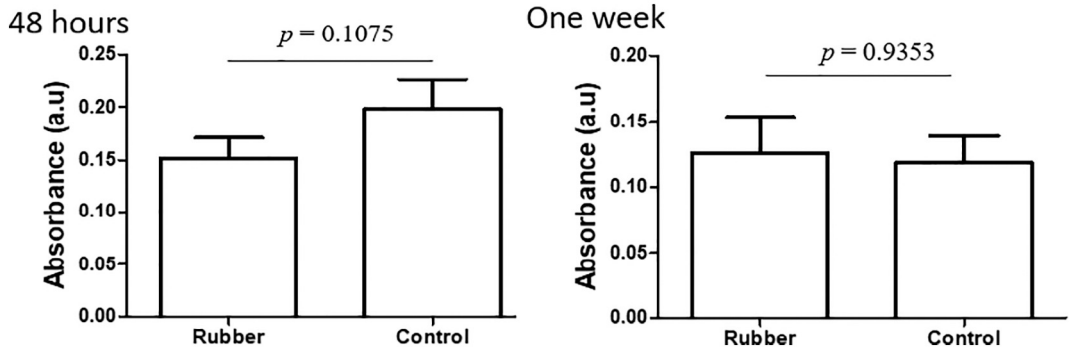

Fig. 7. Average and standard deviation of optical density of stem cell cultures grown on Hybrid NR surfaces and of control cells cultured in the absence of NR for one week. (Results expressed mean ± SEM, n = 12, Mann & Whitney test).

phosphate hybrids (NR-CaP) with particular focus on the morphological and structural characteristics, the physicochemical stability in simulated body fluid (SBF), and also the activity of the coating in forming/precipitating magnesium and calcium phosphate from the SBF medium. The results indicated that the concentration of ammonia and centrifugation velocity (2000*g*, 6000*g*, 10,000*g* and 14,000*g*) have little influence on the chemical structure of the extracted NR cream phase, as evaluated by vibrational spectroscopic techniques (FTIR and Raman). The encapsulation of CaP by NR was attributed mainly to electrostatic interactions between negatively charged biomolecules present in rubber and positively charged CaP particles. We have studied the interaction between NR-CaP hybrids and a simulated body fluid, aiming to access desirable properties to exploit the applications as bioactive coatings. The surfaces were physicochemically modified during 30 days in contact with SBF. The formation of calcium phosphate particles on NR coatings occurs due to the electrostatic interaction between negatively charged layer along the NR surface (−57 mV) and Ca^{2+}, thus inducing the nucleation of Ca-based salts, especially with phosphate ions (PO_4^{3-}). The apatites then grew spontaneously accompanied by consuming the calcium and phosphate ions. Various ions (e.g., Ca^{2+}, $CaOH^{+}$, PO_4^{3-}, HPO_4^{2-}, and CaH_2PO^{4+}) on the surfaces can enable the adsorption ability of the protein and some chemicals in the human body. On the other hand, the hybrid NR-CaP coating formed on Si substrate exhibited biocompatibility, stability and biodegradability in different levels (time dependence). Such properties should open horizons for applications of these hybrids as biomaterials for implants, scaffolds and drug delivery systems.

Acknowledgements

The authors thank the Growth of Crystals and Ceramic Materials team of the Universidade de São Paulo, Victor Teixeira Noronha and Viviane Macedo Saboia of the Universidade Federal do Ceara for all the support in the experiments with simulated body fluid Dr. Hassan Rammal and prof. Dr. Halima Kerdjoudj for all support in the experiments with stem cells. This work was supported by the Brazilian Agency FAPESP, grant number 2013/21970-8 and CAPES Agency.

Appendix A. Supplementary data

Supplementary data to this article can be found online at https://doi.org/10.1016/j.msec.2018.09.048.

References

[1] T.A. Dick, L.A. Dos Santos, In situ synthesis and characterization of hydroxyapatite/natural rubber composites for biomedical applications, Mater. Sci. Eng. 77 (2017) 874–882.
[2] A. Wisutiratanamanee, K. Poochinda, S. Poompradub, Low-temperature particle synthesis of titania/silica/natural rubber composites for antibacterial properties, Adv. Powder Technol. 28 (4) (2017) 1263–1269.
[3] P. Yu, H. He, Y. Jia, S. Tian, J. Chen, D. Jia, Y. Luo, A comprehensive study on lignin as a green alternative of silica in natural rubber composites, Polym. Test. 54 (2016) 176–185.
[4] Y. Zhan, Y. Meng, Y. Li, Electrical properties of binary PVDF/clay and ternary graphite-doped PVDF/clay nanocomposites, Mater. Lett. 192 (2017) 115–118.
[5] M. Ferreira, R.J. Mendonça, J. Coutinho-Netto, M. Mulato, Angiogenic properties of natural rubber latex biomembranes and the serum fraction of *Hevea brasiliensis*, Braz. J. Phys. 39 (2009) 564–569.
[6] C. Ereno, S.A.C. Guimarães, S. Pasetto, R.D. Herculano, C.P. Silva, C.F.O. Graeff, O. Tavano, O. Baffa, A. Kinoshita, Latex use as an occlusive membrane for guided bone regeneration, J. Biomed. Mater. Res., Part A 95 (2010) 932–939.
[7] R.D. Herculano, A.A. De Queiroz, A. Kinoshita, O.N. Oliveira Jr., C.F.O. Graeff, On the release of metronidazole from natural rubber latex membranes, Mater. Sci. Eng. C 31 (2011) 272–275.
[8] E. Abraham, P.A. Elbi, B. Deepa, P. Jyotishkumar, L.A. Pothen, S.S. Narine, S. Thomas, X-ray diffraction and biodegradation analysis of green composites of natural rubber/nanocellulose, Polym. Degrad. Stab. 97 (2012) 2378–2387.
[9] M.M. Araujo, E.T. Massuda, M.A. Hyppolito, Anatomical and functional evaluation of tympanoplasty using a transitory natural latex biomembrane implant from the rubber tree *Hevea brasiliensis*, Acta Cir. Bras. 27 (2012) 566–571.
[10] W. Pichayakorn, J. Suksaeree, P. Boonme, W. Taweepreda, T. Amnuaikit, G.C. Ritthidej, Deproteinised natural rubber used as a controlling layer membrane in reservoir-type nicotine transdermal patches, Chem. Eng. Res. Des. 91 (2013) 520–529.
[11] F.A. Borges, N.R. Barros, B.C. Garms, M.C.R. Miranda, J.L.P. Gemeinder, J.T. Ribeiro-Paes, R.F. Silva, K.A. Toledo, R.D. Herculano, Application of natural rubber latex as scaffold for osteoblast to guided bone regeneration, J. Appl. Polym. Sci. (2017), https://doi.org/10.1002/APP.45321.
[12] J.M.L. Moura, J.F. Ferreira, L. Marques, L. Holgado, C.F.O. Graeff, A. Kinoshita, Comparison of the performance of natural latex membranes prepared with different procedures and PTFE membrane in guided bone regeneration (GBR) in rabbits, J. Mater. Sci. Mater. Med. 25 (2014) 2111.
[13] J.F. Floriano, L.S. Mota, E.L. Furtado, V.J. Rossetto, C.F. Graeff, Biocompatibility studies of natural rubber latex from different tree clones and collection methods, J. Mater. Sci. Mater. Med. 25 (2014) 461–470.
[14] F.A. Borges, E.A. Filho, M.C.R. Miranda, M.L. Santos, R.D. Herculano, A.C. Guastaldi, Natural rubber latex coated with calcium phosphate for biomedical application, J. Biomater. Sci. Polym. Ed. (2015), https://doi.org/10.1080/09205063.2015.1086945.
[15] C.S. Danna, D.G.S.M. Cavalcante, A.S. Gomes, L.E. Kerche-Silva, E. Yoshihara, I.O. Osorio-Román, L.O. Salmazo, M.A. Rodríguez-Pérez, F.R. Aroca, A.E. Job, Silver nanoparticles embedded in natural rubber films: synthesis, characterization and evaluation of in vitro toxicity, J. Nanomater. (2016), https://doi.org/10.1016/j.saa.2011.07.024.
[16] S. Santipanusopon, S.A. Riyajan, Effect of field natural rubber latex with different ammonia contents and storage period on physical properties of latex concentrate, stability of skim latex and dipped film, Phys. Procedia 2 (2009) 127–134.
[17] K. Berthelot, S. Lecomte, Y. Estevez, V. Zhendre, S. Henry, J. Thevenot, E.J. Dufourc, I.D. Alves, F. Peruch, Biochim. Biophys. Acta (2013), https://doi.org/10.1016/j.bbamem.2013.1008.1025.
[18] K. Nawamawat, J.T. Sakdapipanich, C.C. Ho, Y. Ma, J. Song, J.G. Vancso, Colloids Surf. A Physicochem. Eng. Asp. 390 (2011) 157–166.
[19] M.M. Rippel, C.A. Leite, L.T. Lee, F.J. Galembeck, Formation of calcium crystallites in dry natural rubber particles, Colloid Interface Sci. 288 (2005) 449–456.
[20] R.M. Nascimento, F.L. Faita, D.L.S. Agostini, A.E. Job, F.E.G. Guimarães, I.H. Bechtold, Production and characterization of natural rubber – Ca/P blends for biomedical purposes, Mater. Sci. Eng. C 39 (2014) 29–34.
[21] C. Thepchalerm, L. Vaysse, S. Wisunthorn Pansook, S. Kiatkamjornwong, The stability of lutoids in *Hevea brasiliensis* latex influences the storage hardening of natural rubber, J. Rubber Res. 18 (2015) 17–26.
[22] R.M. Nascimento, V.R. Carvalho, J.S. José Silvio Govone, A.C. Hernandes, N.C. Cruz, Effects of negatively and positively charged Ti metal surfaces on ceramic coating adhesion and cell response, J. Mater. Sci. Mater. Med. 28 (2017) 33.
[23] F.J. Lu, S.L. Hsu, A vibrational spectroscopic analysis of the structure of natural rubber, Rubber Chem. Technol. 60 (1987) 647–658.
[24] S. Rolere, S. Liengprayoon, L. Vayssea, J. Sainte-Beuvea, F. Bonfilsa, Investigating natural rubber composition with Fourier Transform Infrared (FT-IR) spectroscopy: a rapid and non-destructive method to determine both protein and lipid contents simultaneously, Polym. Test. 43((2015) 83–93.
[25] Andreas Barth, Infrared spectroscopy of proteins, Biochim. Biophys. Acta Biomembr. Bioenergetics 1767 (2007) 1073–1101.
[26] R.D. Simoes, A.E. Job, D.L. Chinaglia, V. Zucolotto, J.C. Camargo-Filho, N. Alves, J.A. Giacometti, O.N. Oliveira Jr., C.J.L. Constantino, Structural characterization of blends containing both PVDF and natural rubber latex, Raman Spectrosc. 36 (2005) 1118–1124.
[27] F. Lhert, F. Capelle, D. Blaudez, C. Heywang, J. Turlet, Raman spectroscopy of phospholipid black films, Phys. Chem. B 104 (2000) 11704–11707.
[28] B.P. Gaber, W.L. Peticolas, On the quantitative interpretation of biomembrane structure by Raman spectroscopy, Biochim. Biophys. Acta 465 (1977) 260.
[29] R.G. Snyder, S.L. Hsu, S. Krimm, Vibrational spectra in the C−H stretching region and the structure of the polymethylene chain, Spectrochim. Acta 34A (1978) 395.
[30] A. Rygul, K. Majzner, K.M. Marzec, A. Kaczor, M. Pilarczyk, M. Baranska, Raman spectroscopy of proteins: a review, J. Raman Spectrosc. 44 (2013) 1061–1076.
[31] V. Stefova, B. Soptrajanova, F. Spirovskia, I. Kuzmanovskia, H.D. Lutzc, B. Engelenc, Infrared and Raman spectra of magnesium ammonium phosphate hexahydrate (struvite) and its isomorphous analogues. I. Spectra of protiated and partially deuterated magnesium potassium phosphate hexahydrate, J. Mol. Struct. 689 (2004) 1–10.
[32] N.J. Crane, V. Popescu, M.D. Morris, P. Steenhuis, M.A. Ignelzi, Raman spectroscopic evidence for octacalcium phosphate and other transient mineral species deposited during intramembranous mineralization, Bone 39 (2006) 434–442.
[33] G.R. Sauer, R.E. Wuthier, Fourier transform Raman spectroscopy of synthetic and biological calcium phosphates, Calcif. Tissue Int. 54 (1994) 414–420.
[34] C. Vogel, C. Adam, D. Mc Naughton, Determination of phosphate phases in sewage sludge ash-based fertilizers by Raman microspectroscopy, Appl. Spectrosc. 67 (2013) 1101–1105.
[35] H. Rammal, M. Dubus, L. Aubert, F. Reffuveille, D. Laurent-Maquin, C. Terryn, P. Schaaf, H. Alem, G. Francius, F. Quilès, S.C. Gangloff, F. Boulmedais, H. Kerdjoudj, Bioinspired nanofeatured substrates: suitable environment for bone regeneration, ACS Appl. Mater. Interfaces 12; 9 (14) (2017) 12791–12801.
[36] Paterno, L.G.; Peres Junior, J.B.R.; Kramer, J.O.; Pimentel, L.C.; Gomes, N. S. Tratamento do Látex de Borracha Natural com Tanino Vegetal. Patent BR1020170100766, INPI - Instituto Nacional da Propriedade Industrial, Brazil, 2017.
[37] K. Xiao, Y. Li, J. Luo, J.S. Lee, W. Xiao, A.M. Gonik, R.G. Agarwal, K.S. Lam, The effects of surface charge on in vivo biodistribution of PEG-oligocholic acid based micellar nanoparticles, Biomaterials 32 (2011) 3435.